

Review

Progress in Development of Nanostructured Manganese Oxide as Catalyst for Oxygen Reduction and Evolution Reaction

Jing Han Siow¹, Muhammad Roil Bilad^{2,*}, Wahyu Caesarendra², Jia Jia Leam¹, Mohammad Azmi Bustam¹, Nonni Soraya Sambudi¹, Yusuf Wibisono³ and Teuku Meurah Indra Mahlia^{4,*}

¹ Chemical Engineering Department, Universiti Teknologi PETRONAS, Bandar Seri Iskandar 32610, Perak, Malaysia; jhsio53095@gmail.com (J.H.S.); jiajia.leam@gmail.com (J.J.L.); azmibustam@utp.edu.my (M.A.B.); soraya.sambudi@utp.edu.my (N.S.S.)

² Faculty of Integrated Technologies, Universiti Brunei Darussalam, Jalan Tungku Link, Gadong BE1410, Brunei; wahyu.caesarendra@ubd.edu.bn

³ Bioprocess Engineering, Faculty of Agricultural Technology, Universitas Brawijaya, Malang 65141, Indonesia; y_wibisono@ub.ac.id

⁴ Centre for Green Technology, Faculty of Engineering and Information Technology, University Technology Sydney, Sydney, NSW 2007, Australia

* Correspondence: roil.bilad@ubd.edu.bn (M.R.B.); TMIndra.Mahlia@uts.edu.au (T.M.I.M.)

Abstract: The rise in energy consumption is largely driven by the growth of population. The supply of energy to meet that demand can be fulfilled by slowly introducing energy from renewable resources. The fluctuating nature of the renewable energy production (i.e., affected by weather such as wind, sun light, etc.), necessitates the increasing demand in developing electricity storage systems. Reliable energy storage system will also play immense roles to support activities related to the internet of things. In the past decades, metal-air batteries have attracted great attention and interest for their high theoretical capacity, environmental friendliness, and their low cost. However, one of the main challenges faced in metal-air batteries is the slow rate of oxygen reduction reaction (ORR) and oxygen evolution reaction (OER) that affects the charging and the discharging performance. Various types of nanostructure manganese oxide with high specific surface area and excellent catalytic properties have been synthesized and studied. This review provides a discussion of the recent developments of the nanostructure manganese oxide and their performance in oxygen reduction and oxygen evolution reactions in alkaline media. It includes the experimental work in the nanostructure of manganese oxide, but also the fundamental understanding of ORR and OER. A brief discussion on electrocatalyst kinetics including the measurement and criteria for the ORR and the OER is also included. Finally, recently reported nanostructure manganese oxide catalysts are also discussed.

Keywords: nanostructure manganese oxide; sustainable energy technologies; oxygen reduction and evolution reaction; metal-air battery



Citation: Siow, J.H.; Bilad, M.R.; Caesarendra, W.; Leam, J.J.; Bustam, M.A.; Sambudi, N.S.; Wibisono, Y.; Mahlia, T.M.I. Progress in Development of Nanostructured Manganese Oxide as Catalyst for Oxygen Reduction and Evolution Reaction. *Energies* **2021**, *14*, 6385. <https://doi.org/10.3390/en14196385>

Academic Editors: Adriano Sacco and Bashir A. Arima

Received: 4 July 2021
Accepted: 1 October 2021
Published: 6 October 2021

Publisher's Note: MDPI stays neutral with regard to jurisdictional claims in published maps and institutional affiliations.



Copyright: © 2021 by the authors. Licensee MDPI, Basel, Switzerland. This article is an open access article distributed under the terms and conditions of the Creative Commons Attribution (CC BY) license (<https://creativecommons.org/licenses/by/4.0/>).

1. Introduction

The continuous growth of population has led to the increase in energy consumption. Most of the energy demand has been produced through the combustion of fossil fuels. The atmospheric contamination has attracted global attention where various environmental laws and treaties for the control of air pollution [1]. The United Nations has also developed 17 Sustainable Development Goals (SGDs) in 2015 to steer the world towards achieving growth without compromising the environment [2], which encourage the usage of clean and sustainable energy [3]. Renewable energy sources (i.e., solar, wind, biofuels, etc.) have attracted tremendous attention as alternative to supply energy that traditionally comes from combustion of the fossil fuels [4]. With lower emission of anthropogenic gases, renewable energy resources offer promising potential [5–7].

Efficient utilization of energy from renewable resources requires storage systems that are not only safe, but also cost-effective. A robust storage system is highly required to

also support devices related to the Internet of things (IoT) where the use of battery is indispensable. The IoT devices are sometime deployed in remote areas with limited access to electricity grid. Hence, great efforts have been put on development of materials that can be used to fabricate low cost, yet high-performance batteries [8].

One of the batteries that have been receiving great interest is the metal–air batteries, i.e., the zinc-air batteries. Zinc-air batteries are considered the most promising alternatives to enhance renewable source energies for the future storage and release of electrical energy, as they can be quickly refueled with fresh zinc powder and granules. The reactant at the cathode is oxygen which is abundant (from air) and free. Zinc-air batteries also do not require a storage casing which is typically heavy and space consuming. They have received tremendous attention because of the advantage of high specific energy density with a constant discharge voltage. Unlike other metals such as lithium, zinc has very low reactivity, allowing it to be handled safely. Nevertheless, the large overpotential (ΔV) between the oxygen evolution reaction (OER) and the oxygen reduction reaction (ORR) reduces the cycle life and limits its performance [8,9]. Therefore, it is critical to develop suitable catalyst for the OER and ORR to address the issue.

Platinum (Pt) is still the most used catalyst for the ORR and the OER. Yet, commercialization of Pt-based catalyst in zinc-air batteries is still limited by the high cost and the susceptibility to poisoning [10]. Hence, the search for more economic and robust catalysts with high catalytic activities have becoming the main key in the development of the zinc-air batteries. A recent review on catalyst developments for OER and ORR can be obtained elsewhere [11,12]. Among them, manganese oxide is an attractive alternative thanks to its robust OER and ORR performance [10,13–15]. Besides that, its abundance in natural ores, low toxicity, low cost, and environmental friendliness also make it a more attractive choice as the electrocatalyst. However, the unmodified manganese oxide has a weaker affinity to oxygen than the platinum, resulting in a lower catalytic activity [16]. Nonetheless, research has demonstrated that the catalytic performance of manganese oxide for ORR and OER is highly sensitive to its structured. It, thus, opens opportunity for further developments by manipulating the microstructure [17] or through combination of other metals in multi-metal oxides [18].

Over the last decades, the performances of manganese oxide catalysts have been significantly improved through nanoscale modification of their morphologies and structures [19–21]. Hence, this review focuses on the effect of different nanostructures on the electrocatalytic performance of manganese oxide as a bifunctional electrode for ORR and OER in alkaline media. This paper reviews recent developments of the nanostructure manganese oxide and their performance in oxygen reduction and oxygen evolution reactions in alkaline media. A brief discussion on electrocatalyst kinetics including the measurement and criteria for ORR and OER is also included. Finally, recently reported nanostructure manganese oxide catalysts are also discussed.

2. Oxygen Reduction Reaction

The reduction of oxygen at the cathode of a metal air battery is a complex electrochemical reaction. This section briefly overviews the two- and four-electron pathway of the electrochemical reactions to enable good understanding of how a change in morphology of MnO_2 catalyst can dictate the reaction pathway. The reduction of oxygen in alkaline aqueous solution at standard condition (at 1 bar and 25 °C) can be briefly given as in Equations (1)–(6) [22–25]:

For the direct four-electron pathway:



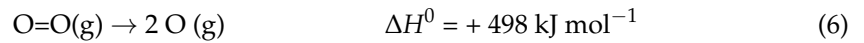
2-electron peroxide reduction pathway:



2-electron peroxide decomposition pathway:



where NHE denotes normal hydrogen electrode. ORR is one of the slowest reactions due to the high bond energy of the oxygen molecule.

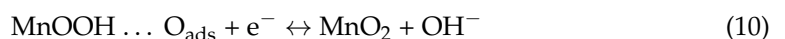
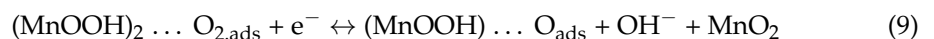
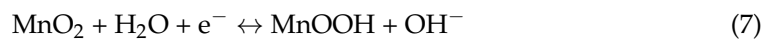


The ORR proceeds either via the 4-electron (4e^-) pathway (Equation (1)) or the 2-electron (2e^-) pathway (Equations (2) and (4)). For the latter, peroxide ions are first produced followed by the reduction (Equation (3)) or disproportionation (Equation (5)) of the peroxide. For carbon electrodes without transition metal catalysts, the peroxide decomposition and reduction reactions are relatively slow [13].

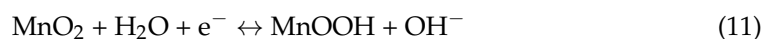
The ORR pathway is highly affected by the adsorption of reacting species on the catalyst active sites. The ORR is a structure-sensitive reaction, as such the structure of the catalyst affects the pathways of ORR, which prompts development of highly porous catalyst [26]. Both binding energy and surface geometry affect oxygen adsorption configuration on the catalyst active sites [27]. The high structure sensitivity allows different pathways of ORR even when using the same type of catalyst, but differ in structure due to the difference in the O_2 adsorption configurations and the O_2 -surface interactions [24]. The O_2 adsorption can proceed either through the bidentate or O_2 adsorption [22,24,25]. For the former, two oxygen atoms coordinate with the catalyst resulting in mainly the direct 4-electron pathway. For the latter, only one oxygen atom perpendicularly coordinates with the catalyst mainly results in the 2-electron pathway with peroxide ions formation. Since the formed peroxide is corrosive and can harm the carbon cathode of a cell which thus affects the stability of the cell, the 4-electrons pathway is more desirable in both the fuel cell and the metal-air battery.

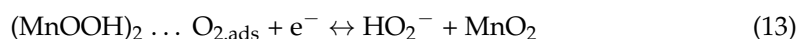
In the ORR reactions with manganese oxide catalyst electrode, oxygen molecules are first dissociated and adsorbed on the catalyst surface. The existence of oxygen vacancies in the manganese oxide facilitates the oxygen adsorption [16]. Several studies have demonstrated that the ORR proceeds on MnO_2 by two main routes as in Equations (7)–(13) [28–30]. In both the four- and the two-electron pathways, manganese dioxide is first converted into manganese oxyhydroxide. During this process, dissociative adsorption of O_2 occurs. The transfer of electron to the adsorbed is considered as the rate-determining step.

i. The complete four-electron reduction pathway;



ii. The two-electron hydrogen peroxide generation pathway.



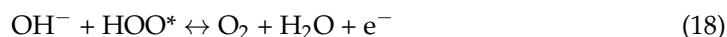
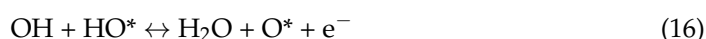


3. Oxygen Evolution Reaction

Oxygen is produced when recharging a secondary zinc-air battery; hence the reaction is named as “oxygen evolution reaction.” The hydroxyl groups (OH^-) in the electrolyte is oxidized and transformed into water and oxygen. The equation and standard half-cell potential at standard condition is stated in Equation (14) [31,32]:



In alkali conditions, OH^- ions attach to the manganese oxide active site to promote an alternative pathway as in Equations (15)–(18) [33].



The surface electrocatalytic activity of metal oxide catalyst is unfortunately a complex reaction. Phase changes are prevalent both at the surface and in the near-surface region that depends greatly on pH and applied potential. Characterization and performance test of MnO_2 showed reasonable and above average performance as a bi-functional catalyst for both the ORR and the OER [22,31,32,34,35]. The compilation of these studies is discussed in Section 5.

4. Electrocatalytic Kinetics for ORR and OER

An electrocatalyst is used to alter the rate of electrochemical reactions by decreasing the activation energy of the charge transfer reaction. In electrocatalyst, the reactant is adsorbed onto the surface of the catalyst to form adsorbed intermediates, which then provide reaction pathways that alter transfer of charges between the reactant and the electrode [20].

The typical technique used for the study of electrocatalytic kinetics can be performed using the 3-electrode set-up which comprises of a potentiostat with a counter Platinum electrode, working and reference electrodes. The representative schematic diagram of the set-up of the potentiostat is shown in Figure 1.

The few important electrocatalytic kinetic parameters required to extract and compare the performance of an electrocatalyst by conducting linear scan voltammetry (LSV) using potentiostat are: (i) onset potential (E_{i0}), (ii) overpotential (η), (iii) current density exchange (i_0), (iv) Tafel slope of anodic and cathodic for both the OER and the ORR and lastly (v) number of electrons transferred in reaction (n) for the ORR. These parameters are critical in providing insightful information to explain the mechanisms of the electrochemical reactions, herein briefly discussed.

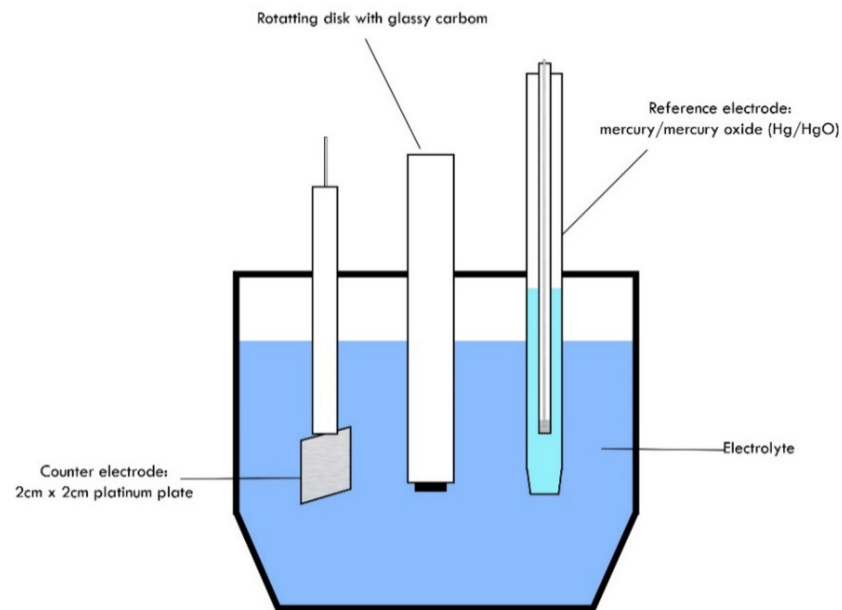


Figure 1. Typical three-electrode set-up for electrochemical characterization for electrocatalyst.

4.1. Onset Potential (E_{i0})

The onset potential describes the energy investment required before the equilibrium system starts to generate or receives the current from or for the reaction. By observing the linear scan voltammetry for the OER and the ORR, onset potential can be easily obtained by determining from the lowest potential for OER and highest potential for ORR at which the reaction product is formed at defined conditions.

4.2. Overpotential (η)

The difference between the reduction potential of theoretical half-reaction thermodynamically and the one observed experimentally at equilibrium is defined as overpotential. It is also referred to as the onset potential value. The theoretical reduction potential can be obtained by the Nernst Equation [36] as shown in Equation (19).

$$E = E^0 - \frac{RT}{nF} \ln \frac{[Ox]}{[Red]} \quad (19)$$

where E^0 is the standard cell potential, R gas constant ($8.314 \text{ J K}^{-1} \text{ mol}^{-1}$), T operating temperature (K), n number of transferred electrons, F the Faraday constant (of $96,485 \text{ C mol}^{-1}$), $[Ox]$ and $[Red]$ refer to the concentration of the oxidized and the reduced species, respectively.

The theoretical reduction potential should be the same as the experimental onset potential value in an ideal condition. However, the applied potential is always much higher than the theoretical reduction potential in the actual cases. Such phenomenon occurs as the extra potential is used to overcome the electrode kinetic barrier or simply dissipates as heat by resistance in the reaction. Hence, by evaluating the overpotential from the onset potential obtained using Equation (20), efficiency and energy lost in the system can be estimated.

$$\eta = E - E_{i0} \quad (20)$$

4.3. Exchange Current Density (i_0)

The cathodic (j_c) and anodic (j_a) currents are equal at equilibrium, where the overpotential (η) equals to 0. Under this equilibrium there is no overall net current. The intercepts value at $\eta = 0$ denotes the exchange current (j_0). Ratio of the exchange current to the area of the electrode is defined as the exchange current density (i_0). Exchange current density is an indicator to compare the interaction of charge transfer between the reactant and the

electrocatalyst [37]. A good electrocatalyst with a high exchange current density for the target reaction usually indicates it has a good electrocatalytic performance. The exchange current density can be used to obtain the Butler-Volmer equation from the Tafel plot.

4.4. Tafel Slope

From the definition of the exchange current density, $i_o = -i_c = i_a$ at $\eta = 0$, the partial anodic and cathodic current densities are the concentration of electroactive-dependent as in Equation (21).

$$i_a = zFk_a[\text{Red}] \quad i_c = zFk_c[\text{Ox}] \quad (21)$$

The rate constants of k_a and k_c change in an exponential manner with the overpotential in the first approximation, where z depicts the number of transferred electrons as shown in Equation (22).

$$k_a = k_{a0} \exp\left(\frac{\alpha_A n F}{RT} \eta\right) \quad \text{and} \quad k_c = k_{c0} \exp\left(\frac{\alpha_C n F}{RT} \eta\right) \quad (22)$$

Through substitution and rearrangement, the Butler-Volmer equation for the overall potential dependence of the current density can be obtained as in Equation (23).

$$i = i_0 \left[\exp\left(\frac{\alpha_A z F}{RT} \eta\right) - \exp\left(\frac{\alpha_C z F}{RT} \eta\right) \right] \quad (23)$$

Then, by rewriting the Butler-Volmer equation to a logarithm function form, a linear relation known as Tafel equation for the anodic (Equation (24)) and the cathodic (Equation (25)) can be obtained:

$$\log_{10}(i) = \log_{10}(i_0) + \frac{\alpha_A z F}{\ln(10) RT} \eta \quad (24)$$

$$\log_{10}(-i) = \log_{10}(i_0) + \frac{\alpha_C z F}{\ln(10) RT} \eta \quad (25)$$

An example of the Tafel plot is shown in Figure 2. By applying Equations (24) and (25), the linear region of the slope can be extrapolated to obtain the exchange current density at y-intercept. Meanwhile, the linear slope which is known as the Tafel slope can be used to calculate the electron transfer coefficient for the cathodic (α_C) and the anodic reaction (α_A) through comparison with Equations (24) and (25). From the Tafel plot, a smaller Tafel slope indicates a higher reaction rate constant, which also represents good electrocatalytic kinetics [38].

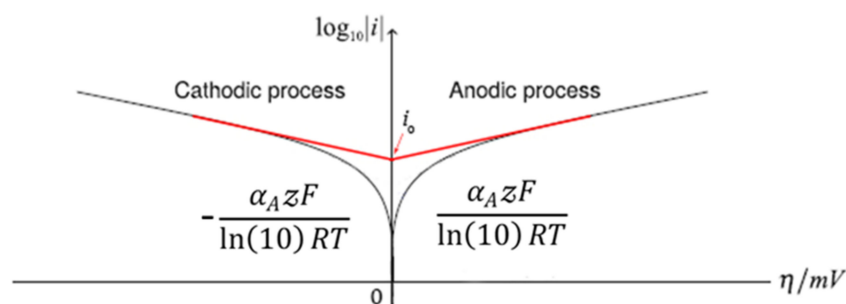


Figure 2. Example of Tafel plot showing a cathodic process in the left side and anodic process on the right side.

4.5. Number of Electrons Transferred for ORR

The electrochemical testing of catalysts for ORR or OER is usually performed by a rotating disk electrode (RDE) or a rotating ring disk electrode (RRDE). It is crucial to use a rotating electrode because the rotation helps draw the solution to gather the oxygen at

the electrode, which thus enables a controlled transport of oxygen to the electrode from the electrolyte solution. The rotations also result in centrifugal forces which transport electrolytes to the centre of the rotating electrode.

For the typical ORR experiments, catalyst suspension in a form of a drop coating of a small aliquot is made by catalyst and binder such as Nafion and PVDF on the carbon surface of the rotating electrode. Meanwhile, oxygen is pumped into the electrolyte solution until saturation before the experiment is started to produce an oxygen saturated electrolyte for oxygen reduction.

The RDE system is used to perform LSV for both ORR and OER, where the current density at the working electrode is monitored as a responding variable of the applied potential, which is scanned from a higher potential to lower potential for reduction or from lower potential to higher potential for oxygen evolution. A typical example of the LSV for ORR polarization curve is shown in Figure 3.

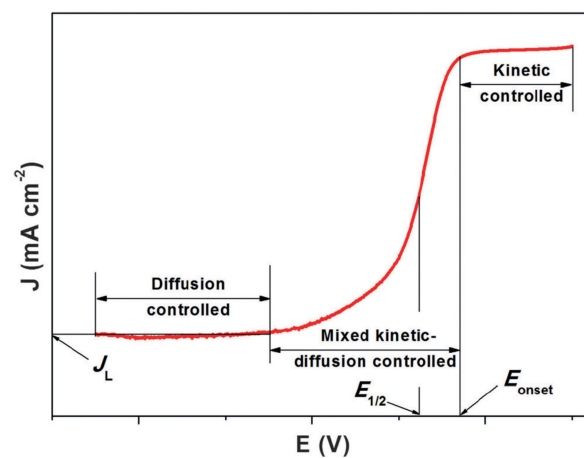


Figure 3. Typical ORR polarization curve. Reprinted with permission from [39]. Copyright 2016 John Wiley and Sons.

Obtaining the number of electrons transferred in LSV of ORR is crucial when studying ORR of an electrocatalyst. By increasing the rotation speed, the flux of oxygen to the electrode increases, the limiting current then becomes more negative. As more oxygen is concentrated at the electrode surface, the cathodic current generated by oxygen reduction is higher. The LSV of different rotational speeds can be analysed by using the Koutecky-Levich equation as in Equation (26).

$$\frac{1}{i} = \frac{1}{i_k} + \frac{1}{i_d} = -\frac{1}{nFAkC^0} - \frac{1}{0.62nFAD_{O_2}^{2/3}v^{-1/6}C^0\omega^{1/2}} \quad (26)$$

where i , i_k , and i_d represent the measured, kinetic, and diffusion-limiting current, n corresponds to the number of electrons transferred in the reduction, F is the Faraday constant, A is the geometric area of the electrode (cm^2), k is the rate constant, C^0 is the saturated concentration of oxygen in the electrolyte which also equals to the solubility of oxygen in the electrolyte, D_{O_2} is the diffusivity of oxygen, v is the kinetic viscosity of solution and ω is the rotational speed in term of angular velocity [23,40–42].

By plotting the linear line of $1/i$ versus $1/\omega^{1/2}$, n can be calculated by using the slope of the Koutecky-Levich line. The number of electrons calculated will indicate the pathway of the ORR reaction that occurs. Further, $n = 4$ indicates predominant mechanisms of the direct 4-electron reduction pathway or the competing apparent of the four-electron process involving the formation and rapid reduction of peroxide. As there will be several complex reactions involving O , OH^- , O_2^- and HO_2^- occurring simultaneously, the calculated n will always be within 2 to 4. Meanwhile, the rate constant of ORR can be calculated by extrapolating the slope to obtain the y-intercept of the Koutecky-Levich line.

5. Effect of Phases of Manganese Oxide Catalyst

By using different synthesis methods, the different phases of manganese oxide can be formed with different properties, including one-dimensional tunneled types, two-dimension layered compound, and three-dimension spinel structure. Table 1 shows all the crystal symmetry, lattice parameters and features of different phases of manganese oxide summarized by Julien and Mauger (2017) [20].

Table 1. Summary of crystallographic data of different manganese dioxide phases, summarized from Julien and Mauger [20].

Compound	Mineral	Crystal Symmetry	Lattice Parameters (Å)	Features
α - MnO_2	Hollandite	Tetragonal ($I4/m$)	a = 9.96; c = 2.85	(2 × 2) tunnel
R - MnO_2	Ramsdellite	Orthorhombic ($Pbnm$)	a = 4.53; b = 9.27; c = 2.87	(1 × 2) tunnel
β - MnO_2	Pyrolusite	Tetragonal ($P4_2/mnm$)	a = 4.39; c = 2.87	(1 × 1) tunnel
γ - MnO_2	Nsutite	Complex tunnel (hex.)	a = 9.65; c = 4.43	(1 × 1)/(1 × 2)
δ - MnO_2	Birnessite	Rhombohedral($R-3m$)	$a_{hex} = 2.94$; $c_{hex} = 21.86$	(1 × ∞) layer
Mg - Bir	Mg-birnessite	Monoclinic ($C2/m$)	a = 5.18; b = 2.84; c = 7.33	(1 × ∞) layer
Na - Bir	Na-birnessite	Monoclinic ($C2/m$)	a = 5.17; b = 2.85; c = 7.32	(1 × ∞) layer
ϵ - MnO_2	Akhtenkite	Hexagonal ($P63/mmc$)	a = 2.85; c = 4.65	Dense stack
λ - MnO_2	Spinel	Cubic ($Fd3m$)	a = 8.04	(1 × 1) tunnel
ψ - MnO_2	Psilomelane	Monoclinic ($P2/m$)	a = 9.56; b = 2.88; c = 13.85	(2 × 3) tunnel
T - MnO_2	Todorokite	Monoclinic ($P2/m$)	a = 9.75; b = 2.85; c = 9.59	(3 × 3) tunnel

Among all the phases of MnO_2 , the α - MnO_2 possesses both (2 × 2) and (1 × 1) tunnels surrounded by double binding octahedral chains. The β - MnO_2 consists of majority (1 × 1) tunnels separated by single chains, and the γ - MnO_2 displays (1 × 1) and (1 × 2) tunnels enveloped in double chains. As reported by Cheng et al. (2012) [24], the performance of ORR activities for different phases follows the sequence: β - MnO_2 < λ - MnO_2 < γ - MnO_2 < α - MnO_2 \approx δ - MnO_2 . Other studies conclude α - MnO_2 as the most active phase of a bifunctional catalyst for both ORR and OER [35,43]. The higher performance of α - MnO_2 is contributed by the high surface concentrations of Mn^{3+} ions due to the low level of impurities and thus high accessibility in this phase compared to others.

6. Effect of Nanosizing on Manganese Oxide

Since both ORR and OER are surface reactions, the electrocatalyst morphology plays an important role in electrocatalytic performance. One of the major reasons for the implementation of the nanosized particle on electrocatalyst is the poor transport properties that cause poor electrochemical performance. According to Julien and Mauger (2017) [20], such poor transport properties are usually caused by the low electronic conductivity and ionic conductivity of the catalyst. By decreasing the particle size, the characteristic time for an electronic species to reach the surface of the catalyst of a fixed dimension can be significantly reduced. At the same time, the surface area of the particle can be significantly increased which thus reduces the resistance of the catalyst.

From previous studies, the physical and chemical properties of MnO_2 nanostructures are found to be highly influenced by their chemical composition, crystallographic structure, as well as particle size and shape [30,32,34,35,44]. The findings were in line with another study [20], where the structure versus property relationship of MnO_2 nanostructures significantly affects the surface area for adsorption of oxygen, thus causing huge differences in performances for bifunctional application of oxygen electrode in alkaline medium. There are several common nanostructures of MnO_2 , such as nanosheets, nanotubes, nanorods, nanowires, nanoflakes, nanoneedles, nanoflowers, nano-urchins and nanosphere [20,30,34,45–47].

7. Electrocatalyst Performance of Nanostructured Manganese Oxide

7.1. Nanoflower

Table 2 summaries the performance of nanostructure manganese oxide catalysts in term of the ORR and the OER parameters. Nanoflower is a newly developed class of

nanoparticles showing structures similar to that of a flower (Figure 4). Nanoflower has gained much attention due to their high stability and high surface area to volume ratio [48]. The typical method for preparation of nanoflower manganese oxide is a hydrothermal method [19,45,49,50]. This procedure is conducted simply by mixing Potassium Permanganate (KMnO_4) and Hydrated Manganese Sulphate ($\text{MnSO}_4 \cdot \text{H}_2\text{O}$) with a ratio of 5:2 dissolved in distilled water transferred into a Teflon-lined pressure autoclave and sent into oil bath or preheated oven with $140\text{ }^\circ\text{C}$ for a dwell time for 2 to 8 h [19,51,52]. Dwell time of 2 h revealed a nanoflower manganese oxide with a Brunauer-Emmett-Teller (BET) surface area of $40.1\text{ m}^2\text{ g}^{-1}$, which are higher than 7.9 and $32.9\text{ m}^2\text{ g}^{-1}$ of bulk particles and nanowires in the work by Cheng et al. (2010) [19] and nanoflower $\alpha\text{-MnO}_2$ of $65.7\text{ m}^2\text{ g}^{-1}$ in the work of Yuan et al. (2015) [53].

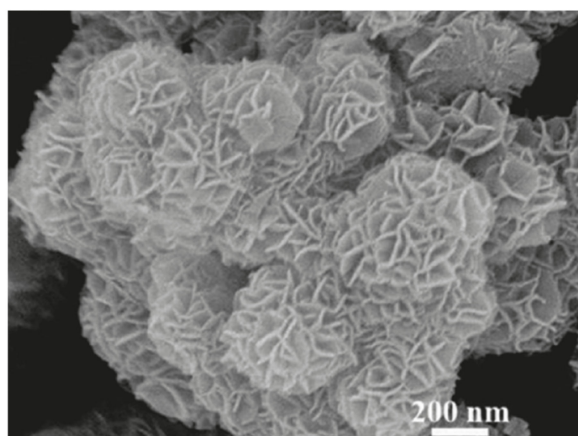


Figure 4. SEM image of a nanoflower $\alpha\text{-MnO}_2$ [19]. Reprinted with permission from [19]. Copyright 2010 American Chemical Society.

In terms of ORR electrocatalyst performance, both works [19,53] have an onset potential around -0.18 V at -1 mA/cm^2 (vs. Ag/AgCl) (Figure 5), giving an overpotential (η) of -0.6 V which is considered as a satisfactory cathode [31]. By calculating the number of electrons transferred by using Koutecky-Levich plot, nanoflower $\alpha\text{-MnO}_2$ has an n -value of 3.7, which is very close to the theoretical value of 4 in the ORR, indicating that the nanoflower $\alpha\text{-MnO}_2$ morphology promotes the ORR to occur by the direct four-electrons pathway to reduce the amount of peroxide ions produced.

In terms of OER electrocatalytic performance, not many studies have been conducted to evaluate the OER performance for a nanoflower manganese oxide. An earlier report [46] states that the $\delta\text{-MnO}_2$ nanoflower has a high overpotential of 0.7 V and low specific surface area of $26\text{ m}^2\text{ g}^{-1}$, proving poor electrocatalytic performance on the OER [31,46]. However, a recent study [53] which embedded $\delta\text{-MnO}_2$ onto carbon-quantum-dots for OER shows an excellent OER electrocatalytic performance. This work manages to synthesis a $\delta\text{-MnO}_2$ with a surface area of $133.85\text{ m}^2\text{ g}^{-1}$. This study reported that the OER for carbon-quantum-dots-embedded $\delta\text{-MnO}_2$ with a high surface area of $254.83\text{ m}^2\text{ g}^{-1}$ has the only overpotential of below 0.2 V and a Tafel slope as low as 43.6 mV dec^{-1} , indicating favorable OER kinetics. However, the results obtained seem to have accuracy due to the high capacitive effect is observed in the LSV as shown in Figure 6. The non-Faradaic region has a current density of $>2\text{ mA/cm}^2$ for all the samples and should be corrected before making a comparison. As there is still a lack of insightful studies available, the OER performance of nanoflowers manganese oxide can be a good subject to be studied in the nearest future for developing MnO_2 bifunctional electrode for energy storage.

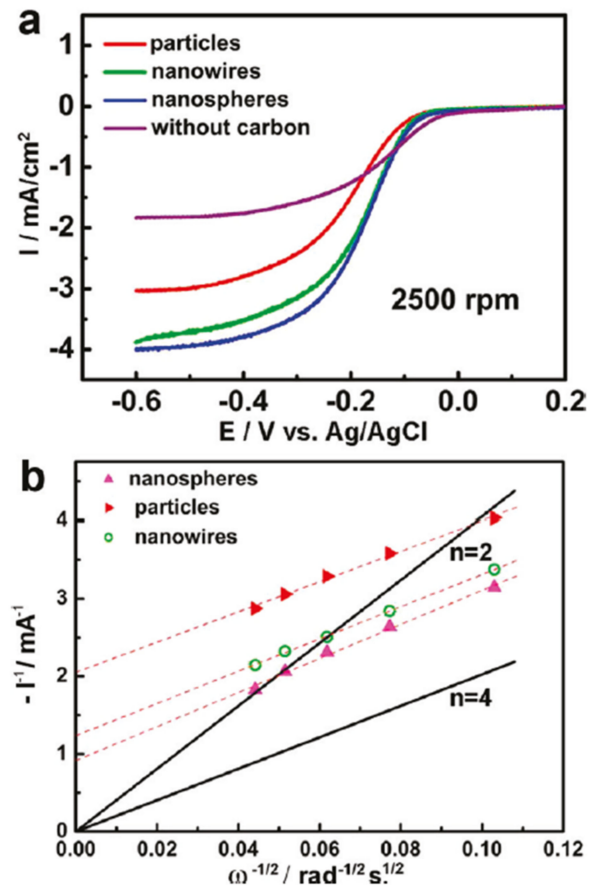


Figure 5. (a) Comparison of the LSV of α -MnO₂ bulk particles, nanowires, nanosphere (nanoflowers) and nanowires without carbon in 0.1M KOH electrolyte at 2500 rpm, and (b) the K-L plot for α -MnO₂ nanospheres (nanoflowers), bulk particles and nanowires at -0.3 V. Reprinted with permission from [19]. Copyright 2010 American Chemical Society.

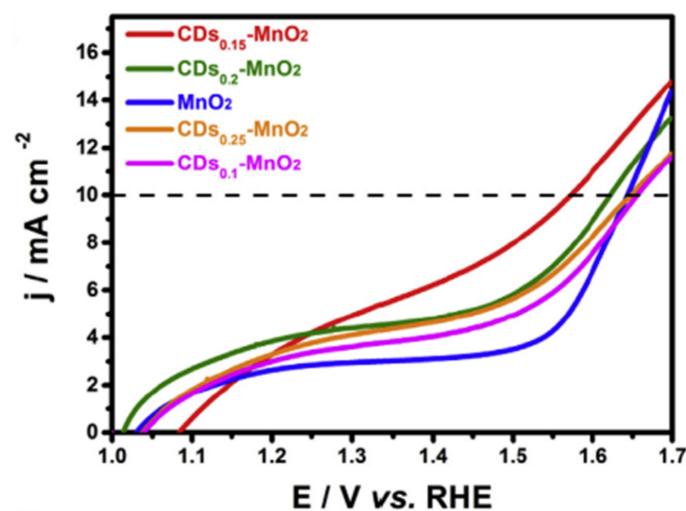


Figure 6. LSV for OER of carbon-quantum-dots-embedded δ -MnO₂ in 1M KOH electrolyte. Reproduced with permission from [53]. Copyright 2019 Elsevier.

7.2. Nanowires

Nanowires are nanostructures with length-to-width ratios greater than 1000 (Figure 7). Similar to nanoflowers, nanowires can also be prepared by the typical hydrothermal

method [20,30,51,54]. The surface area of nanowires nanostructure are usually slightly lower than that of nanoflowers. As reported earlier [30], the α -MnO₂ nanowires had a BET surface area of 27.7 m² g⁻¹ and pore volume of 0.094 cc g⁻¹ which is lower than α -MnO₂ nanoflower of 32.4 m² g⁻¹ and 0.173 cc g⁻¹ respectively.

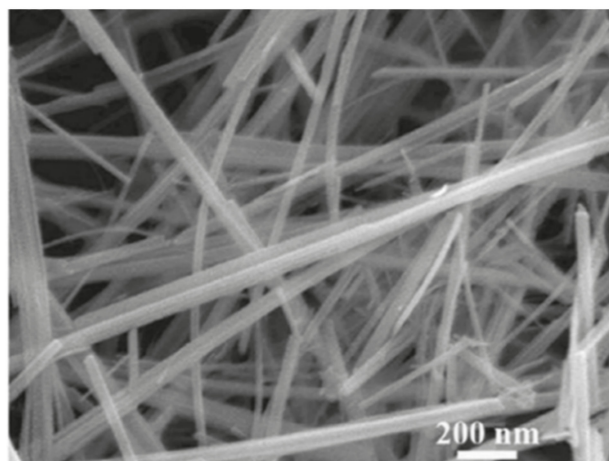


Figure 7. SEM image of α -MnO₂ nanowires. Reprinted with permission from [19]. Copyright 2010 American Chemical Society.

A recent report [30] assessed the ORR electrocatalytic performance and reported *n*-value obtained from K-L plot of α -MnO₂ nanowires of 3.5 while that of α -MnO₂ nanoflowers is 1.9 at -0.8 V. This indicated that the α -MnO₂ nanoflowers did not exhibit its catalytic properties to adsorb oxygen molecules and promoted the ORR to occur via the direct 4-electron pathway. This interpretation was further proven by measuring the % of H₂O₂ produced at -0.8 V. The α -MnO₂ nanowires only yield 3.66% of H₂O₂ production while α -MnO₂ nanoflowers has a H₂O₂ production of 23.89%. Such results disagree with the ones from other studies [19,52]. However, such a phenomenon might be contributed by the different synthesis methods and reagent used. In term of OER electrocatalytic performance, insightful work in evaluating OER of nanowires manganese oxide are still lacking currently.

7.3. Nanorod/Nanotube

Nanorod is a nanostructure that is similar to nanowires, but with a length to width ratio smaller than 20 (Figure 8) that can also be prepared by using the hydrothermal method [30,52].



Figure 8. SEM image of α -MnO₂ nanorod. Reprinted with permission from [30]. Copyright 2015 American Chemical Society.

Selvakumar et al. (2017) [30] reported the surface area of nanorod as $24.8 \text{ m}^2 \text{ g}^{-1}$ with a pore volume of 0.063 cc g^{-1} , much lower than nanowires and nanoflowers. However, another study conducted by [55] shows that the $\alpha\text{-MnO}_2$ nanorod synthesized by electrolysis of KMnO_4 has a high surface area of $59.58 \text{ m}^2 \text{ g}^{-1}$.

In terms of ORR electrocatalytic performance, both works [30,55] show that nanorod exhibits a low n-value from the K-L plot of 1.97 and 3.2, respectively. The difference might be attributed by the different synthesis methods for the manganese oxide, but nanorods have below average electrocatalytic performances in ORR. Full comparison on the morphology and its consequences on the electrocatalyst performances of nanostructured manganese oxide can be seen further in Table 2.

Table 2. Summary of the ORR and OER parameter of recently reported nanostructure manganese oxide catalyst, adapted from [56].

Catalyst	Nanostructure	Electrolyte and Reference Electrode	Synthesizing Method	BET Surface Area (m ² /g)	Overpotential for ORR (mV) at −0.1 mA/cm ²	Electrons Transferred for ORR from K-L Plot	Cathodic Tafel Slope (mV dec ^{−1})	Overpotential for OER (mV) at Specific Density	Anodic Tafel Slope (mV dec ^{−1})	Ref.
α-MnO ₂	Nanoflower	0.1M KOH and Ag/AgCl	Hydrothermal	52.4	−0.570	3.68	-	0.89 at 5 mA/cm ²	-	[56]
α-MnO ₂	Nanoflower/Nanowires			34.9	−0.590	3.31	-	0.91 at 5 mA/cm ²	-	
α-MnO ₂	Nanowires			32.4	−0.530	3.00	-	0.95 at 5 mA/cm ²	-	
α-MnO ₂	Nanoflower	0.1M KOH and Ag/AgCl	Hydrothermal	68.3	−0.302	3.7	-	-	-	[19]
α-MnO ₂	Nanowires			40.1	−0.500	3.87	-	-	-	
α-MnO ₂	Nanowires			27.7	−0.616	3.5	65	-	-	
α-MnO ₂	Nanotubes	0.1M KOH and SCE	Hydrothermal	21.1	−0.586	3.0	90	-	-	[30]
α-MnO ₂	Nanoparticles			34.7	−0.736	2.3	90	-	-	
α-MnO ₂	Nanorod			24.8	−0.606	3.2	65	-	-	
α-MnO ₂	Nanoflower			32.4	−0.876	1.9	115	-	-	
β-MnO ₂	Nanorod	0.1M KOH and Ag/AgCl	Hydrothermal	37.9	−0.75	-	-	-	-	[57]
α-MnO ₂	Nanorod	0.1M KOH and Ag/AgCl	Electrosynthesis	59.58	−0.351	2.23	-	-	-	[55]
α-MnO ₂	Nanoflakes			59.58	−0.651	1.75	-	-	-	
β-MnO ₂	Nanorod	0.1M KOH and SCE	Solid state method	5	−0.551	2.4	-	0.6 at 10 mA/cm ²	180.2	[46]
δ-MnO ₂	Nanoflower		Hydrothermal	26	−0.701	1.7	-	0.75 at 10 mA/cm ²	188.6	
Porous Mn ₂ O ₃	Nanoplates	0.1M KOH and Hg/HgO	Wet-chemical	-	-	-	-	-	81	[34]

8. Conclusions and Perspective

Recent developments on α -MnO₂ nanoflowers and nanowires demonstrate promising performance (i.e., enhanced activity) compared to nanorods or nanotubes structures. To explore a better system to replace the carbon-based fuel system, electrocatalysis for ORR and OER will play an important role in the development of energy storage, especially for metal-air batteries. In terms of ORR catalytic performance, manganese oxide is already well-known as one of the best candidates to replace platinum and there has been great interest in improving the performance of manganese oxide in ORR and preparation method of nanostructure manganese oxide. However, to improve secondary metal-air battery fuel cells, the potential of MnO₂ for OER especially the effect of nanostructure manganese oxide remains unclear even though metal oxide electrocatalyst generally exhibits excellent catalytic abilities for oxygen evolution. Therefore, further studies should involve improvement in the performance of nanostructure manganese oxide in OER to develop a bifunctional catalyst that has an excellent performance in charging and discharging capability. However, the drawback of manganese oxide catalyst is usually their poor electrical conductivity. Hence, future work to evaluate the level of impact of different morphology and surface area on the electrical conductivity should also be conducted. Continuous effort and improvement in the field of renewable energy is required as the driving force to align countries together in achieving sustainable development to meet the needs of the current generation, without compromising the future generations to meet their needs. The availability of reliable battery can accommodate advancements in biofuel [4] and energy-efficient processes reported recently [58,59].

Author Contributions: Conceptualization, M.R.B.; writing—original draft preparation, J.H.S. and M.R.B.; writing—review and editing, J.H.S., J.J.L., M.A.B., N.S.S., Y.W., W.C. and T.M.I.M.; supervision, M.R.B.; All authors have read and agreed to the published version of the manuscript.

Funding: This research received no external funding.

Institutional Review Board Statement: Not applicable.

Informed Consent Statement: Not applicable.

Conflicts of Interest: The authors declare no conflict of interest.

References

1. Höök, M.; Tang, X. Depletion of Fossil Fuels and Anthropogenic Climate Change—A Review. *Energy Policy* **2013**, *52*, 797–809. [[CrossRef](#)]
2. United Nations. *Transforming Our World: The 2030 Agenda for Sustainable Development*; United Nations: New York, NY, USA, 2015; pp. 1–35.
3. Saad, N.; Zainol Ariffin, Z. Implementation of Green Tax in Malaysia: An Exploratory Study. *Growth* **2019**, *6*, 12–19. [[CrossRef](#)]
4. Mahlia, T.M.I.; Syazmi, Z.A.H.S.; Mofijur, M.; Abas, A.E.P.; Bilad, M.R.; Ong, H.C.; Silitonga, A.S. Patent Landscape Review on Biodiesel Production: Technology Updates. *Renew. Sustain. Energy Rev.* **2020**, *118*, 109526. [[CrossRef](#)]
5. Silitonga, A.S.; Shamsuddin, A.H.; Mahlia, T.M.I.; Milano, J.; Kusumo, F.; Siswantoro, J.; Dharmas, S.; Sebayang, A.H.; Masjuki, H.H.; Ong, H.C. Biodiesel Synthesis from Ceiba Pentandra Oil by Microwave Irradiation-Assisted Transesterification: ELM Modeling and Optimization. *Renew. Energy* **2020**, *146*, 1278–1291. [[CrossRef](#)]
6. Silitonga, A.S.; Masjuki, H.H.; Mahlia, T.M.I.; Ong, H.C.; Chong, W.T.; Boosroh, M.H. Overview Properties of Biodiesel Diesel Blends from Edible and Non-Edible Feedstock. *Renew. Sustain. Energy Rev.* **2013**, *22*, 346–360. [[CrossRef](#)]
7. Ong, H.C.; Masjuki, H.H.; Mahlia, T.M.I.; Silitonga, A.S.; Chong, W.T.; Yusaf, T. Engine Performance and Emissions Using Jatropha Curcas, Ceiba Pentandra and Calophyllum Inophyllum Biodiesel in a CI Diesel Engine. *Energy* **2014**, *69*, 427–445. [[CrossRef](#)]
8. Pei, P.; Wang, K.; Ma, Z. Technologies for Extending Zinc–Air Battery’s Cyclelife: A Review. *Appl. Energy* **2014**, *128*, 315–324. [[CrossRef](#)]
9. Li, Y.; Dai, H. Recent Advances in Zinc–Air Batteries. *Chem. Soc. Rev.* **2014**, *43*, 5257–5275. [[CrossRef](#)]
10. Ralph, T.R.; Hogarth, M.P. Catalysis for Low Temperature Fuel Cells. *Platin. Met. Rev.* **2002**, *46*, 117–135.
11. He, H.; Zhang, Y.; Li, Y.; Wang, P. Recent Innovations of Silk-Derived Electrocatalysts for Hydrogen Evolution Reaction, Oxygen Evolution Reaction and Oxygen Reduction Reaction. *Int. J. Hydrog. Energy* **2021**, *46*, 7848–7865. [[CrossRef](#)]
12. Delaporte, N.; Rivard, E.; Natarajan, S.K.; Benard, P.; Trudeau, M.L.; Zaghbi, K. Synthesis and Performance of MOF-Based Non-Noble Metal Catalysts for the Oxygen Reduction Reaction in Proton-Exchange Membrane Fuel Cells: A Review. *Nanomaterials* **2020**, *10*, 1947. [[CrossRef](#)]

13. Yeager, E. Dioxygen Electrocatalysis: Mechanisms in Relation to Catalyst Structure. *J. Mol. Catal.* **1986**, *38*, 5–25. [[CrossRef](#)]
14. Zhou, D.; Lü, X.; Liu, D. Electro-Catalytic Effect of Manganese Oxide on Oxygen Reduction at Teflonbonded Carbon Electrode. *Trans. Nonferrous Met. Soc. China* **2006**, *16*, 217–222. [[CrossRef](#)]
15. Lima, F.H.B.; Calegario, M.L.; Ticianelli, E.A. Electrocatalytic Activity of Manganese Oxides Prepared by Thermal Decomposition for Oxygen Reduction. *Electrochim. Acta* **2007**, *52*, 3732–3738. [[CrossRef](#)]
16. Zhang, T.; Ge, X.; Zhang, Z.; Tham, N.N.; Liu, Z.; Fisher, A.; Lee, J.Y. Improving the Electrochemical Oxygen Reduction Activity of Manganese Oxide Nanosheets with Sulfurization-Induced Nanopores. *ChemCatChem* **2018**, *10*, 422–429. [[CrossRef](#)]
17. Tang, Y.; Zheng, S.; Cao, S.; Xue, H.; Pang, H. Advances in the Application of Manganese Dioxide and Its Composites as Electrocatalysts for the Oxygen Evolution Reaction. *J. Mater. Chem. A* **2020**, *8*, 18492–18514. [[CrossRef](#)]
18. Kim, J.S.; Kim, B.; Kim, H.; Kang, K. Recent Progress on Multimetal Oxide Catalysts for the Oxygen Evolution Reaction. *Adv. Energy Mater.* **2018**, *8*, 1702774. [[CrossRef](#)]
19. Cheng, F.; Su, Y.; Liang, J.; Tao, Z.; Chen, J. MnO₂-Based Nanostructures as Catalysts for Electrochemical Oxygen Reduction in Alkaline Media. *Chem. Mater.* **2010**, *22*, 898–905. [[CrossRef](#)]
20. Julien, C.; Mauger, A. Nanostructured MnO₂ as Electrode Materials for Energy Storage. *Nanomaterials* **2017**, *7*, 396. [[CrossRef](#)] [[PubMed](#)]
21. Liu, X.; Chen, C.; Zhao, Y.; Jia, B. A Review on the Synthesis of Manganese Oxide Nanomaterials and Their Applications on Lithium-Ion Batteries. *J. Nanomater.* **2013**, *2013*, 1–7. [[CrossRef](#)]
22. Yang, D.; Zhang, L.; Yan, X.; Yao, X. Recent Progress in Oxygen Electrocatalysts for Zinc-Air Batteries. *Small Methods* **2017**, *1*, 1700209. [[CrossRef](#)]
23. Mao, L.; Sotomura, T.; Nakatsu, K.; Koshihara, N.; Zhang, D.; Ohsaka, T. Electrochemical Characterization of Catalytic Activities of Manganese Oxides to Oxygen Reduction in Alkaline Aqueous Solution. *J. Electrochem. Soc.* **2002**, *149*, A504. [[CrossRef](#)]
24. Cheng, F.; Chen, J. Metal–Air Batteries: From Oxygen Reduction Electrochemistry to Cathode Catalysts. *Chem. Soc. Rev.* **2012**, *41*, 2172. [[CrossRef](#)] [[PubMed](#)]
25. Spendelov, J.S.; Wieckowski, A. Electrocatalysis of Oxygen Reduction and Small Alcohol Oxidation in Alkaline Media. *Phys. Chem. Chem. Phys.* **2007**, *9*, 2654. [[CrossRef](#)]
26. Jo, H.-G.; Ahn, H.-J. Accelerating the Oxygen Reduction Reaction and Oxygen Evolution Reaction Activities of N and P Co-Doped Porous Activated Carbon for Li-O₂ Batteries. *Catalysts* **2020**, *10*, 1316. [[CrossRef](#)]
27. Speck, F.D.; Santori, P.G.; Jaouen, F.; Cherevko, S. Mechanisms of Manganese Oxide Electrocatalysts Degradation during Oxygen Reduction and Oxygen Evolution Reactions. *J. Phys. Chem. C* **2019**, *123*, 25267–25277. [[CrossRef](#)]
28. Valim, R.B.; Santos, M.C.; Lanza, M.R.V.; Machado, S.A.S.; Lima, F.H.B.; Calegario, M.L. Oxygen Reduction Reaction Catalyzed by e-MnO₂: Influence of the Crystalline Structure on the Reaction Mechanism. *Electrochim. Acta* **2012**, *85*, 423–431. [[CrossRef](#)]
29. Calegario, M.L.; Lima, F.H.B.; Ticianelli, E.A. Oxygen Reduction Reaction on Nanosized Manganese Oxide Particles Dispersed on Carbon in Alkaline Solutions. *J. Power Sources* **2006**, *158*, 735–739. [[CrossRef](#)]
30. Selvakumar, K.; Kumar, S.M.S.; Thangamuthu, R.; Ganesan, K.; Murugan, P.; Rajput, P.; Nath Jha, S.; Bhattacharyya, D. Physicochemical Investigation of Shape-Designed MnO₂ Nanostructures and Their Influence on Oxygen Reduction Reaction Activity in Alkaline Solution. *J. Phys. Chem.* **2015**, *119*, 6604–6618. [[CrossRef](#)]
31. Tahir, M.; Pan, L.; Idrees, F.; Zhang, X.; Wang, L.; Zou, J.-J.; Wang, Z.L. Electrocatalytic Oxygen Evolution Reaction for Energy Conversion and Storage: A Comprehensive Review. *Nano Energy* **2017**, *37*, 136–157. [[CrossRef](#)]
32. Eftekhari, A. Tuning the Electrocatalysts for Oxygen Evolution Reaction. *Mater. Today Energy* **2017**, *5*, 37–57. [[CrossRef](#)]
33. Su, H.-Y.; Gorlin, Y.; Man, I.C.; Calle-Vallejo, F.; Nørskov, J.K.; Jaramillo, T.F.; Rossmeisl, J. Identifying Active Surface Phases for Metal Oxide Electrocatalysts: A Study of Manganese Oxide Bi-Functional Catalysts for Oxygen Reduction and Water Oxidation Catalysis. *Phys. Chem. Chem. Phys.* **2012**, *14*, 14010. [[CrossRef](#)] [[PubMed](#)]
34. Sim, H.; Lee, J.; Yu, T.; Lim, B. Manganese Oxide with Different Composition and Morphology as Electrocatalyst for Oxygen Evolution Reaction. *Korean J. Chem. Eng.* **2018**, *35*, 257–262. [[CrossRef](#)]
35. Mainar, A.R.; Colmenares, L.C.; Leonet, O.; Alcaide, F.; Iruin, J.J.; Weinberger, S.; Hacker, V.; Iruin, E.; Urdanpilleta, I.; Blazquez, J.A. Manganese Oxide Catalysts for Secondary Zinc Air Batteries: From Electrocatalytic Activity to Bifunctional Air Electrode Performance. *Electrochim. Acta* **2016**, *217*, 80–91. [[CrossRef](#)]
36. Fernández-Solis, C.D.; Vimalanandan, A.; Altin, A.; Mondragón-Ochoa, J.S.; Kreth, K.; Keil, P.; Erbe, A. Fundamentals of Electrochemistry, Corrosion and Corrosion Protection. In *Soft Matter at Aqueous Interfaces*; Lang, P., Liu, Y., Eds.; Springer International Publishing: Cham, Switzerland, 2016; Volume 917, pp. 29–70. ISBN 978-3-319-24500-3.
37. Khezri, R.; Hosseini, S.; Lahiri, A.; Motlagh, S.R.; Nguyen, M.T.; Yonezawa, T.; Kheawhom, S. Enhanced Cycling Performance of Rechargeable Zinc–Air Flow Batteries Using Potassium Persulfate as Electrolyte Additive. *IJMS* **2020**, *21*, 7303. [[CrossRef](#)]
38. Suen, N.-T.; Hung, S.-F.; Quan, Q.; Zhang, N.; Xu, Y.-J.; Chen, H.M. Electrocatalysis for the Oxygen Evolution Reaction: Recent Development and Future Perspectives. *Chem. Soc. Rev.* **2017**, *46*, 337–365. [[CrossRef](#)] [[PubMed](#)]
39. Xia, W.; Mahmood, A.; Liang, Z.; Zou, R.; Guo, S. Earth-Abundant Nanomaterials for Oxygen Reduction. *Angew. Chem. Int. Ed.* **2016**, *55*, 2650–2676. [[CrossRef](#)] [[PubMed](#)]
40. Garsany, Y.; Ge, J.; St-Pierre, J.; Rocheleau, R.; Swider-Lyons, K.E. Analytical Procedure for Accurate Comparison of Rotating Disk Electrode Results for the Oxygen Reduction Activity of Pt/C. *J. Electrochem. Soc.* **2014**, *161*, F628–F640. [[CrossRef](#)]

41. Guo, S.; Zhang, S.; Sun, S. Tuning Nanoparticle Catalysis for the Oxygen Reduction Reaction. *Angew. Chem. Int. Ed.* **2013**, *52*, 8526–8544. [[CrossRef](#)]
42. Zhou, R.; Zheng, Y.; Jaroniec, M.; Qiao, S.-Z. Determination of the Electron Transfer Number for the Oxygen Reduction Reaction: From Theory to Experiment. *ACS Catal.* **2016**, *6*, 4720–4728. [[CrossRef](#)]
43. Rossouw, M.H.; Liles, D.C.; Thackeray, M.M. Alpha manganese dioxide for lithium batteries: A structural and electrochemical study. *Mater. Res. Bull.* **1992**, *27*, 10. [[CrossRef](#)]
44. Yang, J.; Xu, J.J. Nanoporous Amorphous Manganese Oxide as Electrocatalyst for Oxygen Reduction in Alkaline Solutions. *Electrochem. Commun.* **2003**, *5*, 306–311. [[CrossRef](#)]
45. Aveiro, L.R.; da Silva, A.G.M.; Antonin, V.S.; Candido, E.G.; Parreira, L.S.; Geonmonond, R.S.; de Freitas, I.C.; Lanza, M.R.V.; Camargo, P.H.C.; Santos, M.C. Carbon-Supported MnO₂ Nanoflowers: Introducing Oxygen Vacancies for Optimized Volcano-Type Electrocatalytic Activities towards H₂O₂ Generation. *Electrochim. Acta* **2018**, *268*, 101–110. [[CrossRef](#)]
46. Meng, Y.; Song, W.; Huang, H.; Ren, Z.; Chen, S.-Y.; Suib, S.L. Structure–Property Relationship of Bifunctional MnO₂ Nanostructures: Highly Efficient, Ultra-Stable Electrochemical Water Oxidation and Oxygen Reduction Reaction Catalysts Identified in Alkaline Media. *J. Am. Chem. Soc.* **2014**, *136*, 11452–11464. [[CrossRef](#)] [[PubMed](#)]
47. Huang, Y.J.; Lin, Y.L.; Li, W.S. Manganese Dioxide with High Specific Surface Area for Alkaline Battery. *Chem. Res. Chin. Univ.* **2012**, *28*, 874–877.
48. Shende, P.; Kasture, P.; Gaud, R.S. Nanoflowers: The Future Trend of Nanotechnology for Multi-Applications. *Artif. Cells Nanomed. Biotechnol.* **2018**, *46* (Suppl. 1), 1–10. [[CrossRef](#)]
49. Yan, D.; Yan, P.X.; Yue, G.H.; Liu, J.Z.; Chang, J.B.; Yang, Q.; Qu, D.M.; Geng, Z.R.; Chen, J.T.; Zhang, G.A.; et al. Self-Assembled Flower-like Hierarchical Spheres and Nanobelts of Manganese Oxide by Hydrothermal Method and Morphology Control of Them. *Chem. Phys. Lett.* **2007**, *440*, 134–138. [[CrossRef](#)]
50. Zhu, G.; Deng, L.; Wang, J.; Kang, L.; Liu, Z.-H. Hydrothermal Preparation and the Capacitance of Hierarchical MnO₂ Nanoflower. *Colloids Surf. A Physicochem. Eng. Asp.* **2013**, *434*, 42–48. [[CrossRef](#)]
51. Haoran, Y.; Lifang, D.; Tao, L.; Yong, C. Hydrothermal Synthesis of Nanostructured Manganese Oxide as Cathodic Catalyst in a Microbial Fuel Cell Fed with Leachate. *Sci. World J.* **2014**, *2014*, 1–6. [[CrossRef](#)]
52. Yuan, H.; Deng, L.; Qi, Y.; Kobayashi, N.; Hasatani, M. Morphology-Dependent Performance of Nanostructured MnO₂ as an Oxygen Reduction Catalyst in Microbial Fuel Cells. *Int. J. Electrochem. Sci.* **2015**, *10*, 14.
53. Tian, L.; Wang, J.; Wang, K.; Wo, H.; Wang, X.; Zhuang, W.; Li, T.; Du, X. Carbon-Quantum-Dots-Embedded MnO₂ Nanoflower as an Efficient Electrocatalyst for Oxygen Evolution in Alkaline Media. *Carbon* **2019**, *143*, 457–466. [[CrossRef](#)]
54. Wang, L.; Duan, G.; Chen, S.-M.; Liu, X. Hydrothermally Controlled Synthesis of α -MnO₂, γ -MnOOH, and Mn₃O₄ Nanomaterials with Enhanced Electrochemical Properties. *J. Alloy. Compd.* **2018**, *752*, 123–132. [[CrossRef](#)]
55. Mahmudi, M.; Widiyastuti, W.; Nurlilasari, P.; Affandi, S.; Setyawan, H. Manganese Dioxide Nanoparticles Synthesized by Electrochemical Method and Its Catalytic Activity towards Oxygen Reduction Reaction. *J. Ceram. Soc. Jpn.* **2018**, *126*, 906–913. [[CrossRef](#)]
56. Jing Han, S.; Ameen, M.; Hanifah, M.F.R.; Aqsha, A.; Bilad, M.R.; Jaafar, J.; Kheawhom, S. Catalytic Evaluation of Nanoflower Structured Manganese Oxide Electrocatalyst for Oxygen Reduction in Alkaline Media. *Catalysts* **2020**, *10*, 822. [[CrossRef](#)]
57. Kumar, N.; Dineshkumar, P.; Rameshbabu, R.; Sen, A. Facile Size-Controllable Synthesis of Single Crystalline β -MnO₂ Nanorods under Varying Acidic Strengths. *RSC Adv.* **2016**, *6*, 7448–7454. [[CrossRef](#)]
58. Osman, A.; Mat Nawi, N.I.; Samsuri, S.; Bilad, M.R.; Shamsuddin, N.; Khan, A.L.; Jaafar, J.; Nordin, N.A.H. Patterned Membrane in an Energy-Efficient Tilted Panel Filtration System for Fouling Control in Activated Sludge Filtration. *Polymers* **2020**, *12*, 432. [[CrossRef](#)]
59. Wan Osman, W.N.A.; Mat Nawi, N.I.; Samsuri, S.; Bilad, M.R.; Khan, A.L.; Hunaepi, H.; Jaafar, J.; Lam, M.K. Ultra Low-Pressure Filtration System for Energy Efficient Microalgae Filtration. *Heliyon* **2021**, *7*, e07367. [[CrossRef](#)] [[PubMed](#)]